PAPER

Magnetic Field Homogeneity of Birdcage Coil for 4 T MRI System with No Lumped Circuit Elements

Ryotaro SUGA[†a)], ***Student Member***, **Kazuyuki SAITO**[††b)], ***Member***, **Masaharu TAKAHASHI**[††], ***Senior Member***, *and* **Koichi ITO**[††], ***Fellow***

SUMMARY In recent years, magnetic resonance imaging (MRI) systems that operate up to under 3 T are being used in clinical practice in Japan. In order to achieve the requirements of higher image quality and shorter imaging times, devices that utilize high magnetic fields (> 3 T) and high power electromagnetic (EM) wave pulses have been developed. The rise of the static magnetic field is proportional to the increase of the EM wave frequency which raises the issue of variation in capacitance used in the radio frequency (RF) coil for MRI system. In addition, increasing power causes problems of withstanding voltage and these approaches leads to generation of non-uniform magnetic field inside the RF coil. Therefore, we proposed a birdcage coil without the use of lumped circuit elements for MRI systems in previous study. However, it is difficult to fabricate this birdcage coil. Hence, simply-structured birdcage coil with no lumped circuit elements is desired. In this paper, we propose a simply-structured birdcage coil with no lumped circuit elements for a 4 T MRI system. In addition, the authors investigated the input impedance and magnetic field distribution of the proposed coil by FDTD calculations and measurements. The results confirm that the proposed birdcage coil matches the performance of the conventional birdcage coil which includes several capacitors.
key words: *magnetic resonance imaging (MRI), birdcage coil, finite-difference time-domain (FDTD) method, biological tissue-equivalent phantom*

1. Introduction

Magnetic resonance imaging (MRI) is being widely used to obtain clear images inside the human body, especially of high water content tissues. The fundamental principle of MR imaging is to receive nuclear magnetic resonance (NMR) signals induced by irradiating the human body placed inside a strong static magnetic field with electromagnetic (EM) wave pulses. The MRI system is composed of various elements including a radio frequency (RF) coil, which plays an essential role in imaging [1]. Several types of RF coils, such as birdcage coils, saddle coils, surface coils, transverse electromagnetic (TEM) coils etc. have been developed and used depending on the body part to be imaged [1]–[4]. These RF coils operate as an antenna that "irradiates the body with EM wave pulses in order to generate NMR signals" and "receiving the NMR signals emitted from the body". This paper focuses on the birdcage coil, which is the most popular type of volume coil. Frequency to emit the NMR signal depends on nucleus properties in human body. It is necessary to use an EM wave in certain specified frequency to emit the NMR signal. Here, frequency of EM fields, f [Hz] is given by the following equation.

$$f = \gamma \cdot B \tag{1}$$

where f is the Lamor precession or resonant frequency of the nucleus [Hz], γ is the gyromagnetic ratio of nuclear [Hz/T]. In the case of water composed of hydrogen atoms, $\gamma = 42.6$ MHz/T. Additionally, B is the magnitude of the static magnetic flux density [T]. In this paper, the authors describe magnetic flux density as magnetic field for reasons of expediency. Thus, frequency to emit NMR signal is directly proportional to the strength of the static magnetic field.

Recent MRI systems that operate at up to 3 T are being used in clinical practice in Japan [5]. In order to achieve the requirement of obtaining more high-quality images and short imaging time, devices, which utilize high magnetic field (> 3 T) and high power EM wave pulses, have been developed [6], [7]. However, some problems caused by high magnetic field and high power EM wave pulses. For instance, the increase of static magnetic field strength causes a rise in the frequency of EM pulses. In such a case, small variability of capacitances used in the birdcage coil, which is one of the most-used volume coils and is loaded a lot of uniform capacitances, will not be ignored. In addition, the use of high power EM pulses will induce breakdown of the capacitances. The improvement of the above problems would increase costs for manufacturing of the coil. It is predicted that these problems are going to become increasingly serious problems when high magnetic field (> 3 T) is utilized with devices for the MRI system. Hence, if we can develop the birdcage coil for MRI system with no lumped circuit elements such as capacitance, it is extremely useful. For this reason, we have developed birdcage coil for MRI system with no lumped circuit element [8]. This birdcage coil has circular conductors which are two different diameters. These conductors were constructed on both surfaces of dielectric cylinder. In this way, this birdcage coil can generate capacitance between circular conductors which are two different diameters. Due to this, birdcage coil does not need any capacitors as lumped circuit elements. However, if conductors on dielectric cylinder are out of position during process of manufacture, characteristics of this birdcage coil become depleted because capacitance changes between some

Manuscript received August 1, 2013.
Manuscript revised November 26, 2013.
[†]The author is with the Graduate School of Engineering, Chiba University, Chiba-shi, 263-8522 Japan.
[††]The authors are with the Center for Frontier Medical Engineering, Chiba University, Chiba-shi, 263-8522 Japan.
a) E-mail: suga@chiba-u.jp
b) E-mail: kazuyuki_saito@faculty.chiba-u.jp
DOI: 10.1587/transcom.E97.B.791

conductors on both surfaces of dielectric cylinder. In other words, it is difficult to fabricate this birdcage coil. Therefore, simply-structured birdcage coil with no lumped circuit elements to reduce manufacturing error is desired.

In this paper, we proposed the simply-structured birdcage coil with no lumped circuit elements to reduce manufacturing error. To be more specific, conductors of the birdcage coil with no lumped circuit elements were constructed on single side surface of dielectric cylinder. It is considered that proposed birdcage coil can be manufactured by technique of making a single side printed circuit board.

2. Calculation Model

2.1 Head Model

Figure 1 show the head model used in the numerical calculation and the experiment. This model is 180 mm in diameter, 250 mm in length and is made of a uniform medium of an average brain tissue [9]. The composition of the phantom for experiment is listed in Table 1. The target values of electrical properties of the phantom are $\varepsilon_r = 58.2$ and $\sigma = 0.49$ S/m at 170 MHz [10]. At 170 MHz, the errors between the target values and the measured electrical constants are 3.4% and 4.1% for relative permittivity ε_r and conductivity σ, respectively. Thus, there is no influence on the birdcage coil performances with such differences.

2.2 Structure of the Birdcage Coil

The RF coil employed in this paper is a birdcage coil for 4 T MRI system. From the Eq. (1), operating frequency of the coil is approximately 170 MHz. Figure 2(a) shows structure of the proposed birdcage coil, previous birdcage coil with no lumped circuit element in Ref. [8] is shown Fig. 2(b) and the conventional birdcage coil is shown Fig. 2(c) for comparison, respectively. Figure 3 shows sectional view of two birdcage coils. The birdcage coil consists of two circular conductors and some conductors which make a connection with circular conductors. The former is called end-ring and the latter is called element. Here, both coils consist of sixteen elements.

Moreover, in order to generate a homogenous magnetic field inside the birdcage coil and control the resonance frequency of the conventional birdcage coil to approximately 170 MHz, a total of thirty two capacitors were attached to the both end-rings of the conventional birdcage coil such as Fig. 2(c). Resonance frequency of the birdcage coil is varied according to the capacitance. In addition, magnetic field distribution inside the coil is varied according to current pattern on elements. For example, to create a homogeneous magnetic field inside cylindrical birdcage coils, the current pattern on a conducting surface should have a sinusoidal dependence on the azimuthal angle of the element location. Please see Ref. [1] for more information about operating principle of the birdcage coil. In this paper, all capacitors have 14.4pF based on an analysis of Birdcage Builder [11] which is computer program provided by Pennsylvania State University. The Birdcage Builder can be used to calculate the current pattern on a conducting surface of element location, and the necessary capacitances of the birdcage coil of a given geometry (diameter of birdcage coil, number of elements, required resonant frequency, and so on) by performing lumped circuit analysis using virtual ground assumptions. In capacitance calculation, each end-ring was treated as a number of segments located between the elements, and the required capacitances were calculated as follows: (1) calculate the current intensity in the leg following the desired current distribution (for example, it will be a sinusoidal distribution in a circular coil design) according to elements angular position, (2) calculate current intensity in the end-ring segments

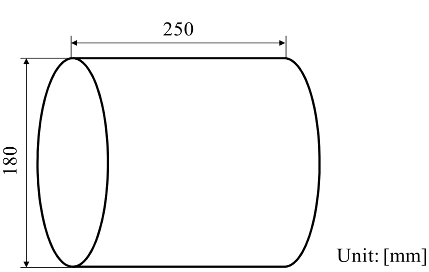

Fig. 1 Head model.

Table 1 Composition of phantom.

Ingredients	Amount [g]
Deionnized Water	3,327.0
Agar	104.6
Sodium Chloride	11.0
Sodium Dehydroacetate	2.0
TX-151	45.2
Polyethylene Powder	250.0

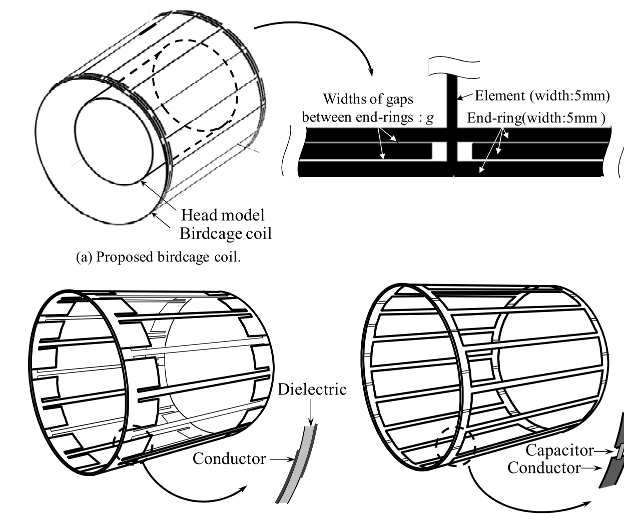

Fig. 2 Birdcage coil.

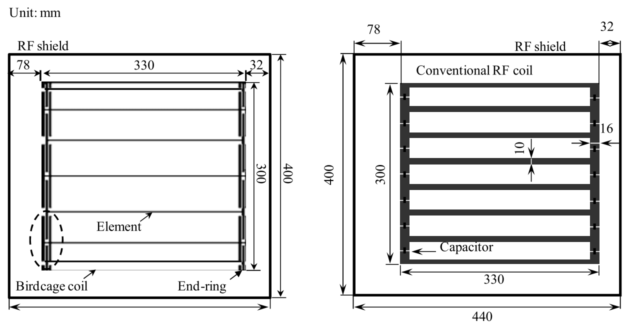

(a) Proposed birdcage coil. (b) Conventional birdcage coil.

Fig. 3 Sectional view of birdcage coils.

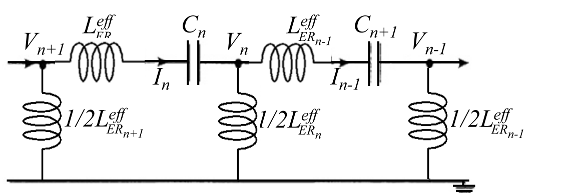

Fig. 4 Circuit model in the birdcage coil for capacitance calculation.

by Kirchhoff's law, (3) calculate the effective inductance of legs concerning the effect of RF shield, (4) calculate the effective inductance of end-ring segments, and (5) calculate the capacitance by performing lumped circuit analysis using Kirchhoff's law. For example, a circuit model for birdcage coil design is shown in Fig. 4. The L^{eff} and L^{eff}_{ER} are the effective inductance of the element and end-ring segment, C is the capacitor inserted on the end-ring segment, I is the current intensity in the end-ring segment, and n is the index.

Figure 2(a) is the proposed birdcage coil without the use of lumped circuit elements. In order to control the resonance frequency of the proposed birdcage coil, gaps are used instead some capacitors such as Fig. 2(a). Therefore, this birdcage coil does not need the capacitor that is the lumped circuit elements. Structure of the proposed birdcage coil is simpler than the coil in Ref. [8] because conductor of Ref. [8] was constructed on both surfaces of dielectric cylinder. Here, end-rings and sixteen elements were constructed on the dielectric pipe ($\varepsilon_r = 2.1$), whose pipe wall thickness is 3 mm.

In this paper, two coils and RF shield are same in size such as Fig. 3(a) and (b). The diameter and the length of both coils are 300 mm and 330 mm each, which is sufficiently large for the head model to be set inside. Additionally, both coils are enclosed in a cylindrical RF shield. The diameter and the length of the RF shield are 400 mm and 440 mm, respectively. All these are composed of metallic sheets. Dimensions of coil and the cylindrical RF shield were determined by Refs. [9], [12], and [13]. In addition, two feeding points were employed in these calculations and the phase difference between them is 90 degree. This excitation method is called "quadrature excitation" and can generate uniform rotate magnetic field inside the birdcage coil.

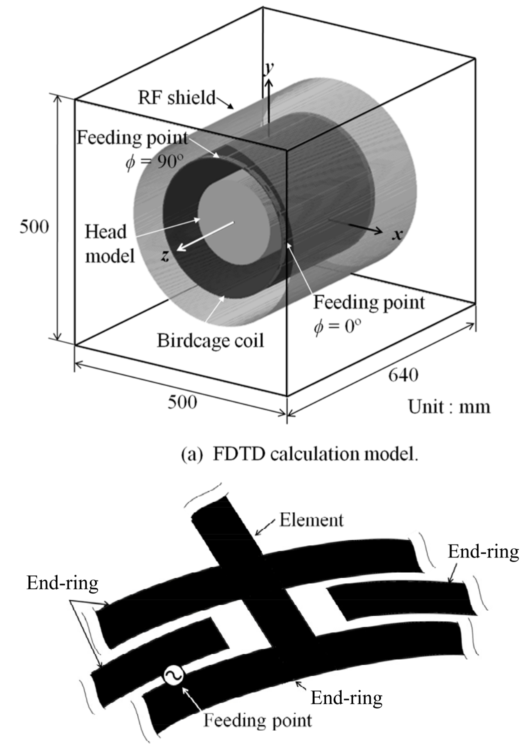

(a) FDTD calculation model.

(b) Enlarged view of around the feeding point of proposed birdcage coil.

Fig. 5 The numerical calculation model consisting of the birdcage coil and the head model (Coordinate origin is center of the coil).

Table 2 The parameters used in FDTD calculations.

Cell size [mm] (minimum)	Δx, Δy	1.0
	Δz	0.2
Cell size [mm] (maximum)	Δx, Δy	5.0
	Δz	5.0
Analytical space [mm^3]		500 × 500 × 640
Time step [ps]		0.641

2.3 Numerical Calculation Model and Conditionsa

In the numerical calculation, the input impedance $|Z|$ at the feeding point of the birdcage coil was calculated by the FDTD method [14], and the magnetic field inside the coil was calculated for comparison with the measurements. The parameters used in FDTD calculations are listed in Table 2.

Figure 5(a) shows the numerical calculation model of the birdcage coil and the head model. The head model is placed in the center of the coil. Figure 5(b) shows enlarged view of around the feeding point of proposed birdcage coil. Feeding points are modeled such as a Fig. 5(b). For the calculation of the input impedance, a derivative Gaussian pulse was excited with 50-Ω internal resistance at the feeding gap at the position $\phi = 0°$. In contrast, a continuous sinusoidal wave was inputted at the feeding gaps at the positions $\phi = 0°$ and $\phi = 90°$ to calculate magnetic field distribution. In order to reduce computational resources, the non-uniform grid FDTD algorithm was adopted. The absorbing boundary condition is 8 layers of Perfectly Matched Layer (PML).

3. Input Impedance of the Proposed Coil

In this paper, in order to adjust the resonant frequency, widths of gaps between end-rings g (see Fig. 2(a)) are changed. Other parameters (e.g. overlap-length between three end-rings, distance between element and center end-ring, and so on) are maintained constant. Figure 6 show relationships between resonant frequency and g. In this paper, impedance-matching of the birdcage coil is not considered because MRI system usually has matching circuit (i.e. we consider only adjust the resonant frequency of the coil.). Moreover, birdcage coil is considered as a parallel resonant circuit as shown in Fig. 4. Generally, a parallel resonant circuit has high impedance at resonant frequency. In other words, absolute value of impedance has local maximum value at resonant frequency. Therefore, absolute value of impedance is shown in this paper because it is only necessary to adjust the resonant frequency. As a result, the resonance frequency was confirmed to be approximately 170 MHz, when widths of gaps are 0.2 mm. Thus, it is considered that proposed coil when widths of gaps are 0.2 mm and conventional coil which are loaded with capacitance of 14.4 pF are equivalent.

In order to compare the measured and calculated input impedances of the proposed birdcage coil containing the head model, when widths of gaps are 0.2 mm are shown in Fig. 7. The continuous line is the calculated result and the broken line is the measured result. The input impedance was calculated at the feeding point at $\phi = 0°$, same as the measured. Here, the measuring instrument was N5230C PNA-L network analyzer by the Agilent Technologies, Santa Clara, California.

As a result, the resonance frequency is confirmed to be approximately 170 MHz. However, slight shifts in resonant frequency and absolute value of impedance between the measured and calculated results were confirmed. These shifts attributed to fabrication error in, such as, the dimension of gaps.

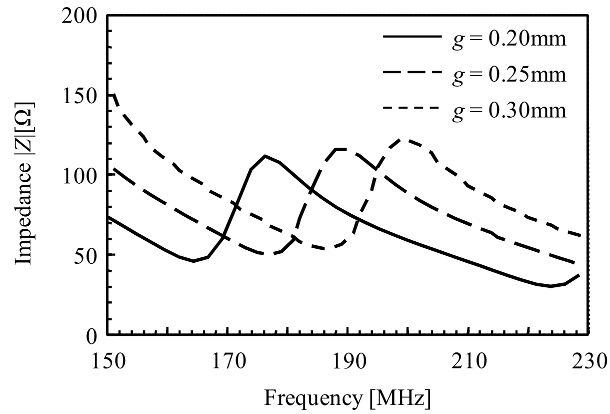

Fig. 6 Input impedance.

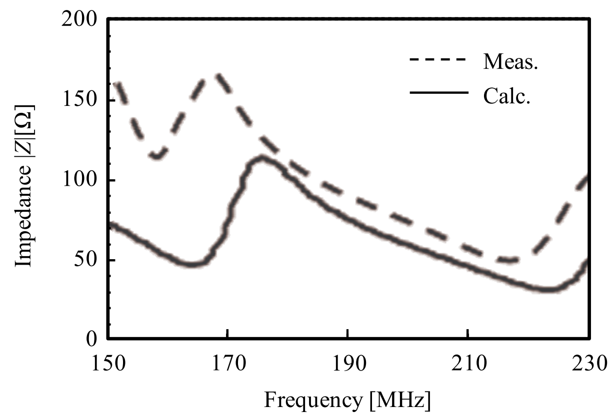

Fig. 7 The measured and calculated input impedance of the proposed coil.

4. Magnetic Field Distribution

It is considered that magnetic field homogeneity in the center of the coil is important because the coil is placed in such a way that target organ is positioned roughly in the center of the coil. In addition, the direction of rotation of the nuclear is radial direction of the coil (i.e. x-y plane). Thus, it is necessary to generate rotate magnetic field in x-y plane. For these reasons, this paper describes the results of magnetic field distributions in x-y plane.

4.1 Calculated Magnetic Field Distribution

Figure 8(a) shows the magnetic field distribution of the proposed coil containing the head model in the x-y plane at center of the coil ($z = 0$ mm). In addition, the magnetic field distribution of the conventional coil containing the head model is shown in Fig. 8(b) for comparison. Here, the magnetic field levels of proposed coil and conventional coil were normalized with equal input power. From these results, it was confirmed that both coils generate uniform magnetic field inside the head model. Figure 9 shows the profiles of magnetic field. The observation line is x axis at $y = 0$ mm in Fig. 8. The continuous line is the result of proposed coil and the broken line is the result of conventional coil. As a result, it was confirmed that the proposed coil has an equivalent uniformity to the conventional birdcage coil. In addition, each component (H_x, H_y and H_z) of magnetic field distributions inside the proposed coil containing the head model is shown in Fig. 10. From these results, we confirmed that level of H_z component, which is parallel to the axial direction of the coil, was small in comparison with the levels of H_x and H_y components. Thus, the spatial phase difference of 90 degrees caused by quadrature excitation between H_x and H_y components of magnetic field distributions were observed. These distributions were observed for a similar result in conventional birdcage coil and it is non-unique characteristics of proposed coil. From these results, it is suggested that the proposed birdcage coil can

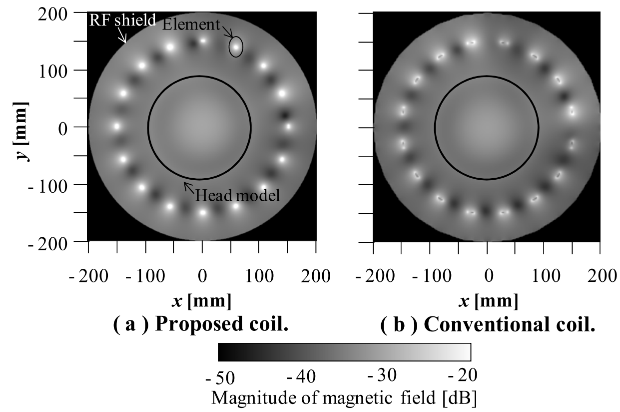

Fig. 8 Magnetic field distribution (absolute value).

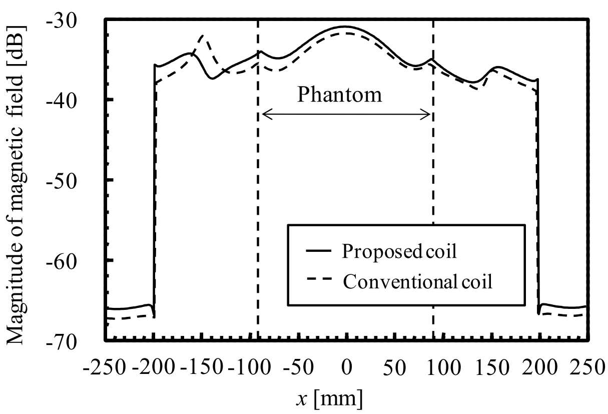

Fig. 9 Profiles of magnetic field (absolute value).

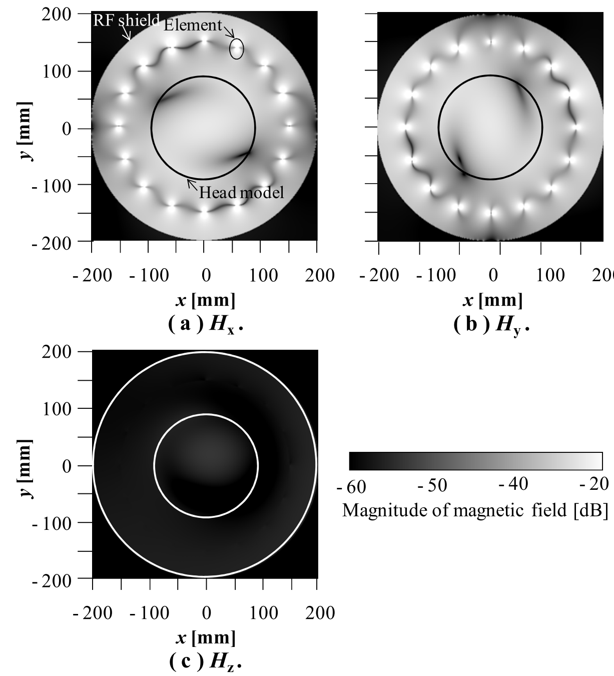

Fig. 10 Magnetic field distribution.

Table 3 Comparison of the average variation δ_{ave}.

Proposed coil	$\delta_{ave} = 0.147$
Conventional coil	$\delta_{ave} = 0.158$

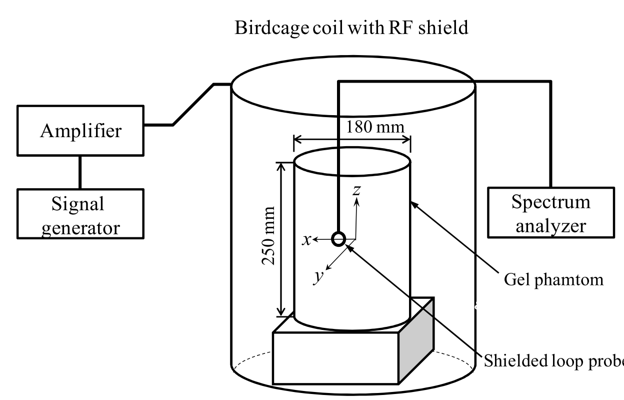

Fig. 11 Setup for measurement of magnetic field distribution.

use for MR imaging. Additionally, in order to compare the magnetic field uniformity inside the head, average variation of the magnetic field inside a head model were calculated by applying the following Eq. (1). The average variation is defined as

$$\delta_{ave} = \frac{1}{SH_{ave}} \iint_S |H - H_{ave}| \, ds \tag{2}$$

where S denotes the circular region [m^2], and H_{ave} denotes average value of H over the region. In this case, S is cross section of the phantom. In addition, range of H_{ave} as defined from 0 to 1. Table 3 illustrates the average variations of magnetic field in the head model for the proposed coil and the conventional coil. The average variation of the proposed coil is approximately $\delta_{ave} = 0.147$, the average variation of the conventional coil is the $\delta_{ave} = 0.158$. As a result, average variation of the conventional coil is slightly larger than the average variation of the proposed coil. However, error of the average variation between the conventional coil and proposed coil was negligible small in terms of practice. Accordingly, it is considered that the proposed birdcage coil has an equivalent homogeneity of magnetic field to the conventional birdcage coil.

4.2 Measurement of the Magnetic Field Distribution

Here, we describe the measurement of the magnetic field distribution inside the human head model and thereby validate the calculated results. Figure 11 shows the experimental setup, where the arrangement of the birdcage coil and human head model is the same as that in Fig. 5. Here, gel phantom is used as a human head model. Gel phantom is filled in dielectric pipe ($\varepsilon_r = 2.1$) and thickness of dielectric pipe is 3 mm. The composition of the gel phantom for measurement of magnetic field distribution is listed

Table 4 Composition of gel phantom.

Ingredients	Amount [g]
Deionnized Water	3,327.0
Sodium Chloride	11.0
Sodium Dehydroacetate	2.0
TX-151	45.2
Polyethylene Powder	250.0

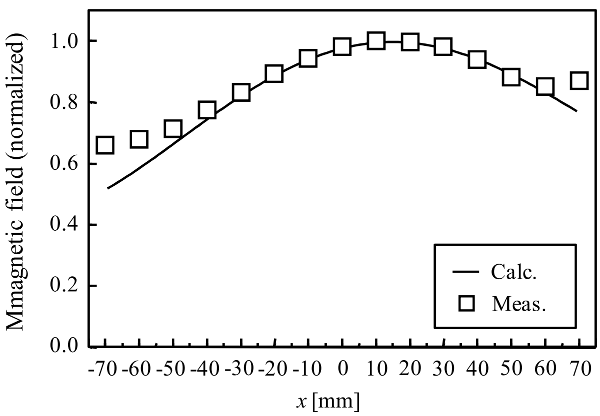

Fig. 12 The measured and calculated magnetic field distribution on the observation line at the position $\varphi = 90°$.

in Table 4. At 170 MHz, the errors between the target values of electrical properties of the gel phantom and the measured electrical constants are less or equal 10% for relative permittivity ε_r and conductivity σ, respectively. Here, the signal was excited at the position $\phi = 0°$ in Fig. 5. The proposed birdcage coil has rotationally-symmetrical structure and equal amplitude signals were exited at two feeding points. From this reason, in the case of 1-port, obtained magnetic field becomes rotation symmetry. Therefore, magnetic field was measured by using 1-port feeding. In order to feed the proposed birdcage coil, a signal generator (8657B Hewlett Packard, Palo Alto, California) and a power amplifier (LA100UF-CE Kalmus, Bothell, Washington) were used. The shielded loop probe was used as the magnetic field probe. Diameter of a shielded loop probe is 5 mm. Then, H_x and H_y were measured by orienting the probe antenna along the x axis at $y = 0$ mm in Fig. 8. Here, the H_z component is omitted because its level is very low as compared to H_x and H_y. A spectrum analyzer (Agilent E4403B) was used to measure the received signal level. The scanning interval on the line was 10 mm. Figure 12 compares the measured and calculated magnetic field distribution on the observation line ($y = z = 0$ mm, $-70 \leq x \leq 70$ mm). The levels are normalized with the maximum value on the observation lines in both cases. The continuous line is the calculated result and square symbols are the measured result. As a result, we confirmed that measurement result disagree with the calculation result in the range of -70 mm $\leq x \leq -50$ mm because the range is noise floor of the spectrum analyzer. However, good agreement was observed between the measured and numerical calculated results of the magnetic field level in the range of $|x| < 50$ mm.

5. Conclusions

This paper proposes a birdcage coil with no lumped circuit elements for 4 T MRI systems; it is an enhanced version of our previous proposal. Conductor of previous birdcage coil was constructed on both surfaces of dielectric cylinder. On the one hand, conductor of proposed birdcage coil was constructed on only one side. Firstly, the authors have clarified the input impedance of the proposed coil by use of FDTD calculations and measurements. The results show that the resonance frequency was approximately 170 MHz, the operating frequency of a 4 T MRI system. Moreover, good agreement was observed between the measured and calculated input impedances.

Secondly, the magnetic field distributions of proposed birdcage coil were investigated. As a result, it was confirmed that the proposed birdcage coil matches the uniformity of the conventional birdcage coil.

Finally, we described the measurement of the magnetic field distribution inside the human head model and thereby validate the numerical calculated results. Good agreement was observed between the measured and calculated results.

The future challenge is to investigate the magnetic field distribution inside a realistic human head model by use of FDTD calculations.

References

[1] J. Jin, Electromagnetic analysis and design in magnetic resonance imaging, CRC Press, Boca Raton, 1998.
[2] M. Fujita, M. Higuchi, H. Tsuboi, H. Tanaka, and T. Misaki, “Design of the RF antenna for MRI,” IEEE Trans. Magn., vol.26, no.2, pp.901–904, March 1990.
[3] T.S. Ibrahim and R. Lee, “Evaluation of MRI RF probes utilizing infrared sensors,” IEEE Trans. Biomed. Eng., vol.53, no.5, pp.963–967, May 2006.
[4] J. Chen, Z. Feng, and J.-M. Jin, “Numerical simulation of SAR and B1-field inhomogeneity of shielded RF coils loaded with the human head,” IEEE Trans. Biomed. Eng., vol.45, no.5, pp.650–659, May 1998.
[5] T. Kawamura, K. Saito, S. Kikuchi, M. Takahashi, and K. Ito, “Specific absorption rate measurement of birdcage coil for 3.0 T magnetic resonance imaging system employing thermographic method,” IEEE Trans. Micro. Theory Tech., vol.57, no.10, pp.2508–2514, Oct. 2009.
[6] T.S. Ibrahim, “A numerical analysis of radiofrequency power requirements in magnetic resonance imaging experiments,” IEEE Trans. Microw. Theory Tech., vol.52, no.8, pp.1999–2003, Aug. 2004.
[7] B.A. Baertlein, Ö. Özbay, T. Ibrahim, R. Lee, Y. Yu, A. Kangarlu, and P.-M.L. Robitaille, “Theoretical model for an MRI radio frequency resonator,” IEEE Trans. Biomed. Eng., vol.47, no.4, pp.535–546, 2000.
[8] K. Saito, T. Kawamura, M. Takahashi, and K. Ito, “Proposition of improve birdcage coil for MRI system with no lumped circuit elements,” IEICE Trans. Commun. (Japanese Edition), vol.J93-B, no.12, pp.1644–1650, Nov. 2010.
[9] T. Kawamura, K. Saito, S. Kikuchi, M. Takahashi, and K. Ito, “Specific absorption rate measurement of birdcage coil for 3.0 T magnetic resonance imaging system employing thermographic method,”

IEEE Trans. Microw. Theory Tech., vol.57, no.10, pp.2508–2514, Oct. 2009.
[10] S. Gabriel, R.W. Lau, and C. Gabriel, "The dielectric properties of biological tissues: II. Measurements in the frequency range 10 Hz to 20 GHz," Phys. Med. Biol., vol.41, pp.2251–2269, April 1996.
[11] C.L. Chin, C.M. Collins, S. Li, B.J. Dardzinski, and M.B. Smith, "BirdcageBuilder: Design of specified — Geometry birdcage coils with desired current pattern and resonant frequency," Concepts in Magnetic Resonance, vol.15, no.2, pp.156–163, Jan. 2002.
[12] J. Chen, Z. Feng, and J.-M. Jin, "Numerical simulation of SAR and B1-field inhomogeneity of shielded RF coils loaded with the human head," IEEE Trans. Biomed. Eng., vol.45, no.5, pp.650–659, May 1998.
[13] U.D. Nguyen, J.S. Brown, I.A. Chang, J. Krycia, and M.S. Mirotznik, "Numerical evaluation of heating of the human head due to magnetic resonance imaging," IEEE Trans. Biomed. Eng., vol.51, no.8, pp.1301–1309, Aug. 2007.
[14] K.S. Yee, "Numerical solution of initial boundary value problems involving Maxwell's equation in isotropic media," IEEE Trans. Antennas. Propag., vol.AP-14, no.3, pp.302–307, May 1966.

Ryotaro Suga was born in Tokyo, Japan, in June 1985. He received the B.E. and M.E. degrees both in electrical engineering from Chiba University, Chiba, Japan, in 2009 and 2011, respectively. He is currently working toward the D.E. degree at Chiba University. His main interests include research on evaluation of the interaction between electromagnetic (EM) field.

Kazuyuki Saito was born in Nagano, Japan, in May 1973. He received the B.E., M.E. and D.E. degrees all in electronic engineering from Chiba University, Chiba, Japan, in 1996, 1998 and 2001, respectively. He is currently an Associate Professor with the Center for Frontier Medical Engineering, Chiba University. His main interest is in the area of medical applications of the microwaves including the microwave hyperthermia. He received the IEICE AP-S Freshman Award, the Award for Young Scientist of URSI General Assembly, the IEEE AP-S Japan Chapter Young Engineer Award, the Young Researchers' Award of IEICE, and the International Symposium on Antennas and Propagation (ISAP) Paper Award in 1997, 1999, 2000, 2004, and 2005 respectively. Dr. Saito is a member of IEEE, the Institute of Image Information and Television Engineers of Japan (ITE), and the Japanese Society for Thermal Medicine.

Masaharu Takahashi was born in Chiba, Japan, on December, 1965. He received the B.E. degree in electrical engineering in 1989 from Tohoku University, Miyagi, Japan, and the M.E. and D.E. degrees both in electrical engineering from Tokyo Institute of Technology, Tokyo, Japan, in 1991 and 1994 respectively. He was a Research Associate from 1994 to 1996, an Assistant Professor from 1996 to 2000 at Musashi Institute of Technology, Tokyo, Japan, and an Associate Professor from 2000 to 2004 at Tokyo University of Agriculture and Technology, Tokyo, Japan. He is currently an Associate Professor at the Center for Frontier Medical Engineering, Chiba University, Chiba, Japan. His main interests are electrically small antennas, planar array antennas, and electromagnetic compatibility. He received the IEEE Antennas and Propagation Society (IEEE AP-S) Tokyo chapter young engineer award in 1994. Dr. Takahashi is a senior member of IEEE, Japan.

Koichi Ito received the B.S. and M.S. degrees from Chiba University, Chiba, Japan, in 1974 and 1976, respectively, and the D.E. degree from Tokyo Institute of Technology, Tokyo, Japan, in 1985, all in electrical engineering. From 1976 to 1979, he was a Research Associate at the Tokyo Institute of Technology. From 1979 to 1989, he was a Research Associate at Chiba University. From 1989 to 1997, he was an Associate Professor at the Department of Electrical and Electronics Engineering, Chiba University, and is currently a Professor at the Graduate School of Engineering, Chiba University. From 2005 to 2009, he was Deputy Vice-President for Research, Chiba University. From 2008 to 2009, he was Vice-Dean of the Graduate School of Engineering, Chiba University. Since April 2009, he has been appointed as Director of Research Center for Frontier Medical Engineering, Chiba University. In 1989, 1994, and 1998, he visited the University of Rennes I, France, as an Invited Professor. He has been appointed as Adjunct Professor to the University of Indonesia since 2010. His main research interests include printed antennas and small antennas for mobile communications, research on evaluation of the interaction between electromagnetic fields and the human body by use of phantoms, microwave antennas for medical applications such as cancer treatment, and antenna systems for body-centric wireless communications. Professor Ito is a Fellow of the IEEE, and a member of AAAS, the Institute of Image Information and Television Engineers of Japan (ITE) and the Japanese Society for Thermal Medicine. He served as Chair of the Technical Group on Radio and Optical Transmissions, ITE, from 1997 to 2001, Chair of the Technical Committee on Human Phantoms for Electromagnetics, IEICE, from 1998 to 2006, Chair of the Technical Committee on Antennas and Propagation, IEICE, from 2009 to 2011, Chair of the IEEE AP-S Japan Chapter from 2001 to 2002, Vice-Chair of the 2007 International Symposium on Antennas and Propagation (ISAP2007), General Chair of the 2008 IEEE International Workshop on Antenna Technology (iWAT2008), Co-Chair of ISAP2008, an AdCom member for the IEEE AP-S from 2007 to 2009, an Associate Editor for the IEEE Transactions on Antennas and Propagation from 2004 to 2010, a Distinguished Lecturer for the IEEE AP-S from 2007 to 2011, and General Chair of ISAP2012. He currently serves as Chair of the IEEE AP-S Committee on Man and Radiation (COMAR), and a Councilor to the Asian Society of Hyperthermic Oncology (ASHO). He has been elected as a delegate to the European Association on Antennas and Propagation (EurAAP) since 2012.